Public health effects of long-term exposure to mobile source PM in California

Center for Transportation, Environment, and Community Health
Final Report

by
M.J. Kleeman

September 29, 2021

DISCLAIMER

TECHNICAL REPORT STANDARD TITLE PAGE

1. Report No.	2.Government Accession No.	3. Recipient's Catalog No.
4. Title and Subtitle **Public health effects of long-term exposure to mobile source PM in California**		5. Report Date September 29, 2021 6. Performing Organization Code
7. Author(s) M.J. Kleeman (ORCID ID #0000-0002-0347-7512)		8. Performing Organization Report No.
9. Performing Organization Name and Address Department of Civil and Environmental Engineering University of California, Davis 1 Shields Avenue Davis, CA, 95616		10. Work Unit No. 11. Contract or Grant No. 69A3551747119
12. Sponsoring Agency Name and Address U.S. Department of Transportation 1200 New Jersey Avenue, SE Washington, DC 20590		13. Type of Report and Period Covered Final Report 10/01/2019 – 03/31/2021 14. Sponsoring Agency Code US-DOT
15. Supplementary Notes		

16. Abstract

$PM_{2.5}$ mass concentration fields associated with on-road motor vehicles were created with 1-km spatial resolution for four heavily polluted urban areas in California: Los Angeles, San Francisco, Sacramento, and Fresno. Monthly-average concentration fields were created for the years 2000 through 2011. Concentration fields were predicted with a Chemical Transport Model (CTM) based on meteorology fields predicted by the Weather Research and Forecast (WRF) model and emissions fields predicted based on measured activity combined with emissions measurements and spatial surrogates. Statistical bias correction was applied to bring predicted $PM_{2.5}$ concentrations into close agreement with measured values. Averaged across all years, motor vehicle tailpipe emissions generally accounted for less than 5% of the total $PM_{2.5}$ concentrations. $PM_{2.5}$ mass concentrations across the study regions decreased by 10-20% between the years 2000-2011, with similar declines predicted for motor vehicle tailpipe contributions to $PM_{2.5}$. The BenMAP-CEv1.5 model created by US EPA estimates that reductions in $PM_{2.5}$ emitted from motor vehicles between 2000-2011 avoids 300 deaths each year with an equivalent monetary value estimated at \$2.3B yr^{-1}. Future studies may use the air pollution exposure fields developed in the current project to analyze health disparities across different population segments or to search for epidemiological associations between pollutant concentrations and health effects.

17. Key Words	18. Distribution Statement
Chemical Transport Model, Exposure Fields, PM2.5, BenMAP	Public Access *[and if applicable, additional outputs (e.g. publications, IP, etc.)]*

19. Security Classif (of this report)	20. Security Classif. (of this page)	21. No of Pages	22. Price
Unclassified	Unclassified		

Form DOT F 1700.7 (8-69)

1 Introduction

Meaningful air pollution regulation in the United States began in California with the creation of the Los Angeles County Air Pollution Control District (LACAPCD) that had the authority to regulate emissions that contributed to "smog" across the cities within its boundaries. Early actions by the LACAPCD limited emissions from factories, orchards, refuse burning, petrochemical refining, and motor vehicles. Authority for regulating emissions from motor vehicles has evolved extensively in the following decades, with significant reductions achieved through numerous advancements in vehicle engine and emissions control technology. California and Los Angeles are still synonymous with "car culture", but the conventional wisdom that motor vehicles dominate air pollution in California is gradually fading.

Accurately estimating the evolving public health impacts of air pollution associated with motor vehicles (or any major pollution source) requires the estimation of accurate pollutant concentration fields across the study region of interest. Traditional air pollution studies relied on measurements at monitoring locations combined with source apportionment studies based on "chemical fingerprints" for this exposure analysis. More recent studies have adapted chemical transport models (CTMs) to estimate exposure fields. CTMs simulate the emissions, transport, deposition, and chemical transformation of pollutants in the atmosphere. CTMs are often used to developed state implementation plans (SIPs) that will achieve compliance with National Ambient Air Quality Standards (NAAQS). Sufficiently accurate CTMs can also be used to estimate pollution concentration fields to estimate public health impacts.

The chief components of photochemical "smog" are ozone (O_3) and airborne particulate matter with aerodynamic diameter smaller than 2.5 μm ($PM_{2.5}$). Of these two components, $PM_{2.5}$ typically accounts for more than 90% of the public health impacts in modern air pollution episodes in the United States. $PM_{2.5}$ spatial gradients are often gradual across major urban areas, making it possible to find associations with public health based on a small number of centralized monitors. Estimating specific health impacts associated with sources such as motor vehicles that are concentrated along transportation corridors is more challenging, because spatial gradients for pollutants emitted around these facilities change much more quickly than total $PM_{2.5}$ concentrations. CTMs developed for the continental US or entire states often use spatial resolutions of 36-km or 12-km that mask many of these important spatial gradients.

The purpose of this project is to predict concentrations fields of $PM_{2.5}$ emitted from on-road motor vehicles with spatial resolution of 1-km in order to resolve sharp spatial gradients around major transportation corridors. CTMs will be developed for four heavily polluted urban areas in California: Los Angeles, the San Francisco Bay Area, Sacramento, and Fresno over the years 2000-2011. Predicted pollutant concentrations will be compared to all available measurements to confirm the accuracy of the model results (and to correct biases when necessary). Source-tagging methods will then be used to predict concentration fields associated with tailpipe emissions from on-road diesel and gasoline vehicles. Once exposure fields are processed, the evolution of the public health impacts of $PM_{2.5}$ emitted from on-road motor vehicles will be estimated using standard tools developed by the US EPA. Final results will estimate the avoided mortality and monetary value of the public health benefits associated with reduced vehicle emissions over the 12-year study period.

2 Methods

2.1 Chemical Transport Model

Simulations for the years 2000-2011were carried out across California using the source-oriented UCD/CIT regional air quality model. The UCD/CIT airshed model is a reactive 3-D CTM that predicts the evolution of gas and particle phase pollutants in the atmosphere in the presence of emissions, transport, deposition, chemical reaction, and phase change as represented by Eq. (1)

$$\frac{\partial C_i}{\partial t} + \nabla \cdot uC_i = \nabla K \nabla C_i + E_i - S_i + R_i^{gas}(C) + R_i^{part}(C) + R_i^{phase}(C) \qquad \text{(eq 1)}$$

where C_i is the concentration of gas or particle phase species i at a particular location as a function of time t, u is the wind vector, K is the turbulent eddy diffusivity, E_i is the emissions rate, S_i is the loss rate, R_i^{gas} is the change in concentration due to gas-phase reactions, R_i^{part} is the change in concentration due to particle-phase reactions and $R_i^{phase}$is the change in concentration due to phase change [1]. Loss rates include both dry and wet deposition. Phase change for inorganic species occurs using a kinetic treatment for gas-particle conversion [2] driven towards the point of thermodynamic equilibrium [3]. Phase change for organic species is also treated as a kinetic process with vapor pressures of semi-volatile organics calculated using the 2-product model [4].

The basic capabilities of the UCD/CIT model are similar to the CMAQ model maintained by the US EPA, but the UCD/CIT model has several source apportionment features and more particle size resolution, which makes it attractive for the current project. The UCD/CIT model explicitly tracks the mass and the number concentration of particles in 15 discrete size bins spanning the range from 10nm through 10 μm, with tracer species used to quantify source contributions to the primary particle mass in each bin. A moving sectional bin approach is used [5] so that particle number and mass can be explicitly conserved with particle diameter acting as the dependent variable.

The emissions of particle source tracers are empirically set to be 1% of the total mass of primary particles emitted from each source category, so they do not significantly change the particle radius and the dry deposition rates. For a given source, the simulated concentration of artificial tracer directly correlates with the amount of PM mass emitted from that source in that size bin. The corresponding number concentration attributed to that source can be calculated using Eq. (2)

$$num_i = \frac{tracer_i \times 100}{\frac{\pi}{6} Dp^3 \rho} \qquad \text{(eq 2)}$$

where $tracer_i$ represents the artificial tracer mass in size bin i, Dp is the core particle diameter, and ρ is the core particle density. Core particle properties are calculated by removing any condensed species to better represent the properties of the particles when they were emitted. More details describing the source apportionment technique in UCD/CIT model are provided in previous studies [6-10].

A total of 50 particle-phase chemical species are included in each size bin. Gas-phase concentrations of oxides of nitrogen (NOx), volatile organic compounds (VOCs), oxidants, ozone, and semi-volatile reaction products were predicted using the SAPRC-11 chemical mechanism [11].

UCD/CIT Model Predictions at 24km, 4km, and 1km resolution

Air pollution exposure fields vary in space and time but the highest concentrations are fundamentally linked to emissions, which are generally correlated with population density. Spatial gradients for many primary pollutants are sharpest around the emissions sources in large cities. This exposure pattern motivates the development of nested exposure fields with coarse spatial resolution in rural areas and fine spatial resolution in urban areas to efficiently describe air pollution exposures across large regions.

Figure 1 illustrates the nested domains used to predict monthly-average PM2.5 concentrations across California in the years 2000-2011in the current project. The outer domain in white uses 24-km resolution to cover all of California, followed by nested domains in cyan that use 4-km resolution to cover central and southern-California, followed by nested domains in yellow that use 1-km resolution to cover Los Angeles, Fresno, Sacramento, and the San Francisco Bay Area. Finer spatial resolution reveals hotspots over smaller regions, which exposes the smaller population within those regions to higher concentrations. The strategy using nested exposure fields with finer spatial resolution over large population centers is an efficient approach to estimating population exposures that balances accuracy with computational expense.

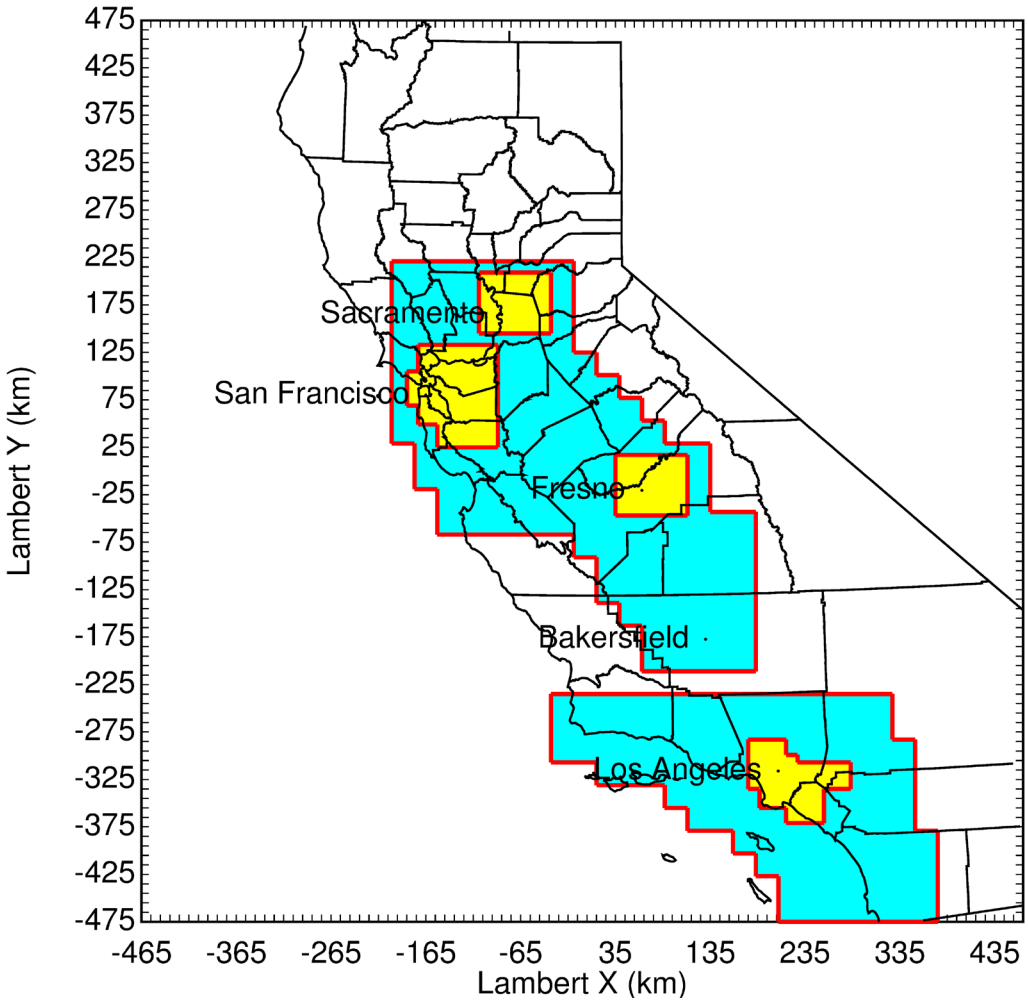

Figure 1: 24-km (white), 4-km (cyan), and 1-km (yellow) model domains used to predict airborne particulate matter concentrations over California during the period 2000-2011.

2.2 Meteorological Model

Hourly meteorology inputs to drive the regional chemical transport model at 24-km, 4-km,. and 1-km resolution in the years 2000-2011 were simulated using the Weather Research and Forecasting (WRF) v3.4 model (www.wrf-model.org). WRF model vertical resolution was 31 vertical layers from the ground level to the top pressure of 100 hPa. Initial and boundary conditions for meteorological simulations were be taken from North American Regional Reanalysis (NARR), which has a spatial resolution of 32 km and a temporal resolution of 3 h. The Yonsei University (YSU) boundary layer vertical diffusion scheme [12] and Pleim-Xiu land surface scheme [13] were adopted in this study. Four-dimensional data assimilation was applied to anchor the model predictions to observed meteorological patterns. Surface friction velocity (u*) was increased by 50% to correct bias during the events with low surface winds that produce the highest pollutant concentrations.

2.3 Emissions

The emission inventories used in the current study were provided by the California Air Resources Board for the years 2000 and 2010. Area and point source emissions between these anchor years were scaled using statewide factors obtained for each individual Emissions Inventory Code (EIC) from https://www.arb.ca.gov/app/emsinv/fcemssumcat/fcemssumcat2016.php unless otherwise discussed below.

Basecase fugitive dust emissions were replaced by an online dust model [14] based on the wind speed, and soil moisture predicted by the WRF model. This change corrects the positive bias in dust emissions and PM2.5 mass noted by Hu et al. [15, 16].

Emissions inventories provided by CARB had spatial resolution of 4-km. Area source emissions with spatial resolution of 1-km were created for major UFP sources using spatial surrogates processed with the "Spatial Allocator" software maintained by US EPA. Off-road gasoline emissions used spatial surrogate 620 (service and commercial employment; 11% of emissions) and spatial surrogate 630 (service and commercial employment at schools, golf courses, and cemeteries; 60% of emissions). Spatial surrogate 620 was created from information provided by Metropolitan Planning Organizations (MPOs) / Council of Governments (COGs) throughout California. Spatial surrogate 630 was obtained directly from CARB at 1km resolution since the corresponding shapefile contained proprietary information. Off-road diesel engines used spatial surrogate 490 (rail lines; 60% of emissions) and 500 (rail yards; 11% of emissions).

Additional details of the methods used to prepare emissions inventories are described below.

2.3.1 Mobile Source Emissions

Mobile source emissions at 24-km and 4-km resolution were obtained from CARB based on calibrated travel demand models combined with California's Emissions Factor (EMFAC) model v2014. EMFAC was also used to scale mobile source emissions in 69 regions throughout California using day-specific meteorology from WRF. Scaling factors were derived for each region by comparing EMFAC results from the anchor year to results from the target year. These factors simultaneously account for emissions changes caused by the year-specific evolving vehicle fleet distribution and emissions changes caused by day-specific meteorology. The unique scaling factors for each of the 69 EMFAC regions were applied to all of the 24-km and 4-km model grid cells contained in that region.

Mobile source emissions at 1-km resolution were calculated using the fuel-based gridded inventory described by McDonald et al. [17] for the year 2005. This inventory provides space- and time-varying values of gasoline and diesel fuel consumption (mass of fuel burned per unit time) by on-road vehicles. McDonald and Harley [18] report that gasoline and diesel fuel sales in the San Francisco Bay Area air basin decreased by 10.5% and 8.1%, respectively, between the years 2005 and 2010. The 2005 gridded fuel-based inventory is scaled accordingly to account for fuel use changes between years 2005 and 2010. Similar corrections are made for the SoCAB inventory in 2010. The EMFAC model was used to calculate emission factors (mass of pollutant emitted per mass of fuel burned) for the pollutants listed in Table 1 and Table 2 for summer and winter, respectively. Fuel consumption values from the fuel-based inventory are multiplied by these emission factors to obtain emission rates (mass of pollutant emitted per unit time).

Table 1. EMFAC summer emission factors (mass of pollutant emitted per mass of fuel burned) for the year 2010. Values in parenthesis were measured in 2010 at the Caldecott tunnel, CA and are provided for comparison.

Pollutant	San Francisco Bay Area		South Coast Air Basin		
	Gasoline Engines	Diesel Engines	Gasoline Engines	Diesel Engines	Units
CO_2	3.0 (3.0)[a]	3.1 (3.2)[a]	2.95	3.2	kg kg^{-1}
CO	29 (14.3)[b]	5.1 (8)[c]	24.5	6.8	g kg^{-1}
NO_x	2.7 (1.9)[b]	24 (28)[c]	2.3	24.8	g kg^{-1}
SO_x	30	30	29.5	29.3	mg kg^{-1}
NMOC (exhaust)	1.4	1.2	1.2	1.6	g kg^{-1}
NMOC (evaporative)	1.6	0	1.5	0	g kg^{-1}
PM_{25}	27 (38)[b]	650	25.5	744	mg kg^{-1}

[a]: values calculated from carbon content of fuels reported by [19]; [b]: values from [20] [c]: values from [21]

Table 2. EMFAC winter emission factors (mass of pollutant emitted per mass of fuel burned) for on-road sources for the year 2010. Values in parenthesis were measured in 2010 at the Caldecott tunnel, CA and are provided for comparison.

Pollutant	San Francisco Bay Area		South Coast Air Basin		
	Gasoline Engines	Diesel Engines	Gasoline Engines	Diesel Engines	Units
CO_2	3.0 (3.0)[a]	3.1 (3.2)[a]	2.95	3.2	kg kg^{-1}
CO	34 (14.3)[b]	5.2 (8)[c]	25.1	7.1	g kg^{-1}
NO_x	3.6 (1.9)[b]	25 (28)[c]	2.6	25.8	g kg^{-1}
SO_x	30	30	29.8	29.3	mg kg^{-1}
NMOC (exhaust)	1.9	1.2	1.3	1.6	g kg^{-1}
NMOC (evaporative)	1.5	0	1.7	0	g kg^{-1}
PM_{25}	29 (38)[b]	660	26.0	751	mg kg^{-1}

[a]: values calculated from carbon content of fuels reported by [19]; [b]: values from [20] [c]: values from [21]

The EMFAC model does not provide emission data for ammonia. Ammonia emissions were estimated by multiplying NOx emission estimates by observed NH_3 to NOx ratios in gasoline and diesel vehicles exhaust plumes. The Fuel Efficiency Automobile Test (FEAT) Data Center reports emission measurements from on-road studies conducted at a variety of locations and time. At each location, the mol fractions of CO, CO_2, HC, NO, SO_2, NH_3, and NO_2 in the exhaust plumes of passing vehicles are measured using remote sensing techniques. Data reported for California sites (Table 3 and Tale 4) collected for 2008 – 2012 were used to calculate average NH3 to NOx emission ratios of 0.19 for on-road gasoline vehicles and 0.0092 for on-road diesel vehicles.

Table 3. Measurement sites from the Fuel Efficiency Automobile Test Data used to calculate NH_3 to NO_x emission ratios for on-road vehicles in the SoCAB.

	Site	Years in the range 2008 to 2012 with available data
Gasoline:	West Los Angeles, LaBrea Boulevard	2008
	Van Nuys	2010
	San Jose	2008
	Fresno	2008
Diesel:	Port of Los Angeles	2008, 2009, 2010, 2012
	Orange County, Riverside Freeway	2008, 2009, 2010, 2012

Table 4. Measurement sites from the Fuel Efficiency Automobile Test Data used to calculate NH_3 to NO_x emission ratios for on-road vehicles in the San Francisco Bay Area.

	Site	Years in the range 2008 to 2012 with available data
Gasoline:	San Jose	2008
	Fresno	2008
	West Los Angeles, LaBrea Boulevard	2008

	Site	Years in the range 2008 to 2012 with available data
	Van Nuys	2010
Diesel:	Port of Los Angeles	2008, 2009, 2010, 2012
	Orange County, Riverside Freeway	2008, 2009, 2010, 2012

Diurnal profiles from McDonald et al. [17] were used to distribute emissions in time, separately for gasoline and diesel (Figure 2). Separate diurnal profiles were used for the following day-of-week scenarios, as reported by McDonald et al. [17]: Monday through Thursday, Friday, Saturday, and Sunday. Daily emission totals were also scaled for each season and each day-of-week scenario, using values reported by McDonald et al. [17]. For example, the gasoline-related CO2 emission total on a Monday is different from the gasoline-related CO2 emission total on a Saturday. Seasonal scaling factors were calculated using data for June through August (summer) and December through February (winter). McDonald et al. [17] provide separate profiles for urban and rural roadway segments but urban profiles were used everywhere to avoid discontinuities where urban grid cells are adjacent to rural grid cells. Fuel densities (gasoline: 741 g L−1; diesel: 850 g L−1) reported by Gentner et al. [19] are used for conversion between volumes and masses of fuel.

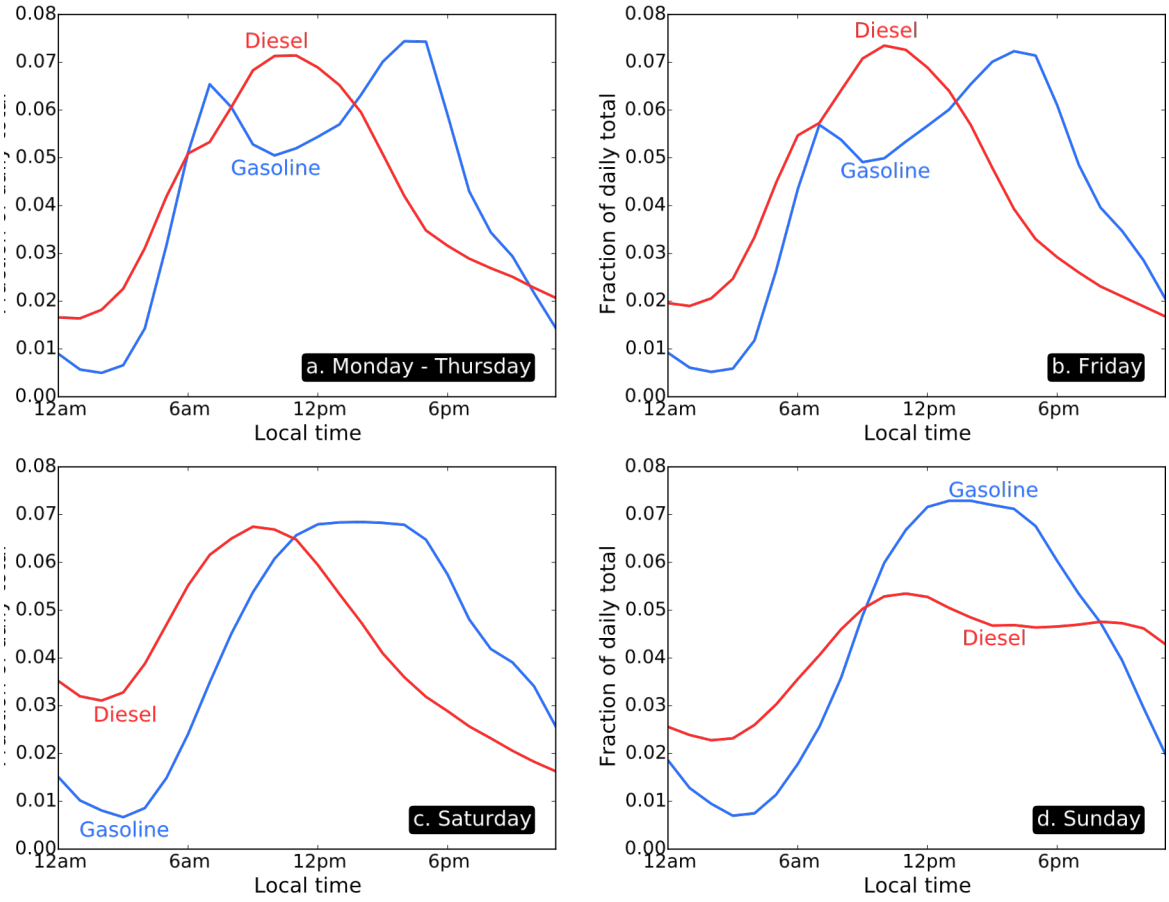

Figure 2: Diurnal emission profiles of on-road vehicle emissions from McDonald *et al.* [17].

2.3.2 Diesel Particle Filters

Diesel particle filters (DPFs) reduce particulate matter emissions from diesel engines by +98% by oxidizing all of the carbonaceous material contained in the particles [22]. The EMFAC v2014 model was used to scale on-road diesel emissions to account for the adoption of DPFs using the procedures described in the previous section. EMFAC describes PM emissions rates but does not account for the change in the composition of emitted particles. The PM emissions from diesel engines equipped with a DPF have low carbon content and higher concentrations of residual components such as sulfate [22]. These changes are important when viewed per unit of emitted PM mass, but fleet average emissions profiles are dominated by the diesel vehicles that do not have DPFs installed. The majority of the effect from DPF adoption was therefore captured by the EMFAC scaling, with a minor contribution from the altered diesel PM profile for the residual ~2% of PM emissions.

2.3.3 Gasoline Direct Injection Engines

Gas Direct Injection (GDI) gasoline vehicles were assumed to penetrate the light duty vehicle fleet starting in 2007 based on market share information. GDI vehicles have higher PM emissions rates and higher EC content than corresponding PFI vehicles. EMFAC accounts for the change in PM emissions rates associated with GDI adoption but not for the resulting change in the composition of emitted particles. In the current study, modified PM emissions profiles for on-road gasoline vehicles were constructed for each simulation year using measurements from Port Fuel Injection (PFI) and GDI vehicles weighted by market share.

2.3.4 Residential Wood Burning

Residential wood smoke emissions were updated by considering POA evaporation and wood burning control policies applied in California [23]. These updates reduced the effective residential wood smoke primary organic aerosol (POA) emissions by 50% in all years compared to the basecase inventories, and better represent long-term trends in wood smoke emissions. $PM_{0.1}$ measurements and source apportionment studies {Xue, 2018 #23}strongly suggest that particulate organic carbon emitted from biomass combustion is semi-volatile, with roughly 50% of the emissions evaporating under typical ambient conditions. In the current study, the OC emitted in wood smoke was reduced by 50% to represent the effects of this evaporation process. The 50% of the residual wood smoke OC that did not evaporate after atmospheric dilution was assumed to be non-volatile in the UCD/CIT calculations.

2.3.5 Natural Gas Combustion

Natural gas combustion exhaust was tracked separately in model calculations to quantify the contributions that this source makes to ambient ultrafine particulate matter. Natural gas emissions were scaled each year based on statewide consumption data available from the United States Energy Information Administration (www.eia.gov). Figure 3 summarizes the natural gas scaling factors applied to the year 2000 emissions to represent the years 2000-2009. Residential and Commercial / Industrial natural gas combustion emissions both peak during the colder winter months. Residential natural gas combustion emissions decrease significantly during warmer summer months due to the decline in heating demand. Commercial / industrial natural gas combustion emissions also decrease during the summer but not as severely as residential emissions. Natural gas emissions for electricity production increase during the summer as demand for air conditioning increases with warmer temperatures.

Natural gas combustion emissions in years 2010 and later were represented using the month of year and day of week emissions presented in the preceding anchor emissions inventory.

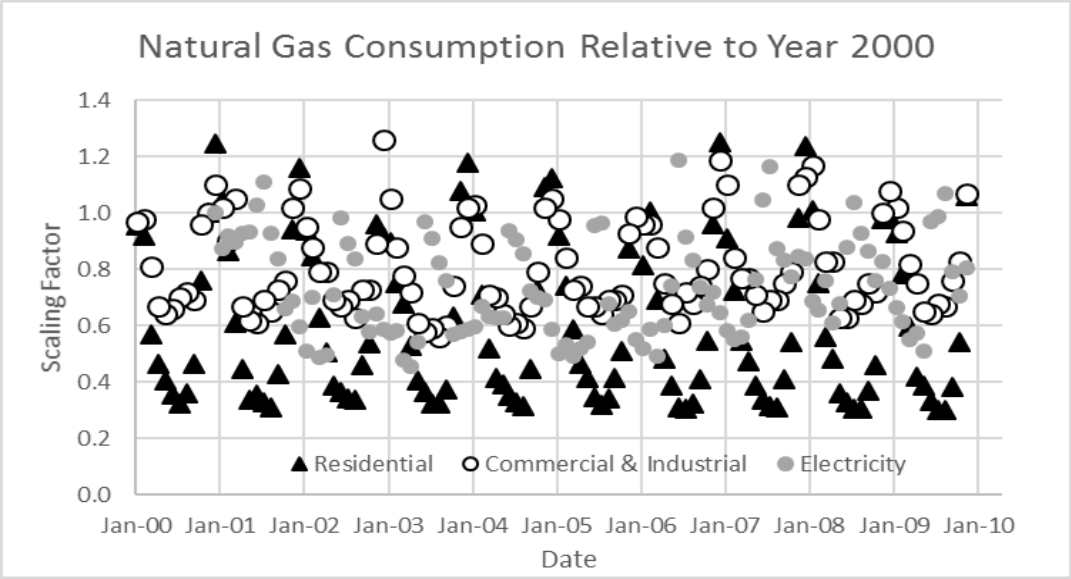

Figure 3: Natural gas scaling factors applied to year 2000 emissions for each target year. Information from the United States Energy Information Administration.

The size distribution of natural gas emissions was measured in laboratory experiments to confirm the accuracy of the source profiles used in model calculations [24]. Emissions dilution experiments indicated that residential natural gas combustion particles will partially evaporate after release to the atmosphere. Residential natural gas particle emissions were reduced by 70% to represent the effects of this evaporation process. The residual natural gas combustion OC was assumed to be non-volatile in the UCD/CIT model calculations.

2.3.6 Soil NOx

Candidate soil NOx emissions were included in the calculations based on a biogeochemical model combined with fertilizer application rates [25]. Soil NOx emissions varied by month of the year based on the effects of temperature on the biogeochemical cycle. Sensitivity studies carried out across years between 2000 – 2015 indicate the inclusion of soil NOx emissions improves the accuracy of model predictions for gas phase ozone and particulate nitrate [26].

2.3.7 Biogenic Emissions

Biogenic emissions were generated using the Model of Emissions of Gases and Aerosols from Nature (MEGANv2.1) based on the meteorological fields generated using the WRF model. The gridded geo-referenced emission factors and land cover variables required for MEGAN calculations were created using the MEGANv2.1 pre-processor tool and the ESRI_GRID leaf area index and plant functional type files available at the Community Data Portal [27].

2.3.8 Wildfires

Daily values of wildfire emissions were generated using the Global Fire Emissions Database (GFED) [28]. Wildfire emissions were assigned the same particle size and composition distribution as routine biomass combustion. Typical wildfire plumes rise to 6-10 km in the atmosphere depending on the intensity of the fire and the local meteorological conditions [29]. Wildfire plumes were injected at the top of the model domain at a height of approximately 5 km in the current simulations. Future studies will evaluate the sensitivity of the plume-rise treatment but this analysis is beyond the scope of the current report.

Wildfire emissions were represented using the Global Fire Emissions Database (GFED) [30]. GFED uses satellite images of burned areas combined with vegetation maps to estimate smoke released each day during wildfires. Spatial resolution of GFED emissions inventories are 0.25 degrees. Smoke from these fires impacted cities throughout central California as plumes were trapped within the Central Valley. Wildfire emissions were assigned particle size and composition profiles based on measurements during biomass burning experiments [31].

2.4 Initial / Boundary Conditions

Initial and boundary conditions for 24-km simulations were generated from the global concentration field predicted by the Model for Ozone and Related chemical Tracers (MOZART). Additional details of MOZART simulations are provided by Emmons et al. [32]. Initial and boundary conditions for nested 4-km and 1-km simulations were obtained from the parent simulations (see Figure 1).

3 Results

3.1 Statistical Bias Correction of Concentration Fields

Predicted monthly-averaged $PM_{2.5}$ concentrations were compared to measured $PM_{2.5}$ concentrations at all available monitoring sites (n=38) across each of the four 1-km study domains for the entire duration of the study period years 2000-2011. Summary statistics were calculated to characterize CTM performance, including the correlation coefficient (R), mean fractional error (MFE), mean fractional bias (MFB), mean error (ME), mean bias (MB), and root mean square error (Table 5). Basecase $PM_{2.5}$ predictions were reasonably well correlated with measured concentrations (average R^2=0.69) but the predicted concentrations exceeded measured concentrations by a factor of approximately 50% (average MFB=0.56). This over-prediction is likely caused by an under-prediction of vertical mixing and dilution associated with the combination of updates to the WRF model v3.4 and the incorporation of non-local transport terms into the aerosol advection / diffusion algorithms.

Table 5. Model performance statistics for basecase simulations followed by statistical bias correction during post-processing. All comparison statistics are based on monthly-averages over the years 2000-2011. Each row represents results from a monitoring site within the indicated 1-KM resolution study domain.

	Basecase								bias_corr_v2						
	Mean obs	R	mfe	mfb	me	Mb	Model pred	rmsqe	R	mfe	mfb	me	mb	Model pred	Rmsqe
FRESNO	17.77	0.85	0.52	0.50	14.13	13.87	31.64	19.67	0.78	0.26	-0.15	5.01	-2.46	15.31	7.81
	16.74	0.81	0.54	0.52	14.02	13.76	30.49	18.94	0.68	0.34	-0.25	5.41	-3.78	12.96	8.15
	17.01	0.86	0.49	0.48	12.39	12.23	29.24	16.80	0.75	0.40	-0.35	5.86	-4.97	12.01	8.45
	20.81	0.85	0.34	-0.26	4.91	-3.15	17.66	6.25	0.02	1.00	-1.00	13.74	-13.74	6.37	15.70
Los Angeles	16.46	0.49	0.57	0.57	12.58	12.42	28.88	13.94	0.74	0.21	0.10	3.28	1.31	17.79	4.16
	18.21	0.48	0.54	0.54	13.03	12.91	31.12	14.71	0.80	0.16	-0.02	2.88	-0.71	17.50	3.83
	17.97	0.61	0.65	0.65	16.84	16.84	34.81	17.80	0.85	0.13	-0.02	2.24	-0.24	17.72	2.94
	14.23	0.41	0.49	0.49	9.14	8.98	23.21	11.24	0.71	0.20	0.09	2.91	1.08	15.30	3.61
	19.43	0.51	0.50	0.50	13.17	13.17	32.60	15.48	0.86	0.12	0.03	2.36	0.29	19.69	3.11
	13.31	0.78	0.70	0.70	15.38	15.38	28.69	16.84	0.62	0.20	-0.05	2.62	-0.70	12.61	3.21

	Basecase								bias_corr_v2						
	Mean obs	R	mfe	mfb	me	Mb	Model pred	rmsqe	R	mfe	mfb	me	mb	Model pred	Rmsqe
	22.26	0.69	0.33	0.32	8.58	8.39	30.65	10.26	0.79	0.14	-0.02	3.22	-0.82	21.38	4.33
	14.95	0.77	0.68	0.68	15.79	15.79	30.74	16.73	0.79	0.15	0.03	2.18	0.33	15.28	2.68
	15.42	0.55	0.63	0.62	13.47	13.43	28.84	14.50	0.85	0.19	0.15	2.88	2.18	17.62	3.53
	15.86	0.64	0.65	0.65	14.98	14.98	30.84	16.29	0.82	0.18	0.11	2.96	1.56	17.41	3.76
	13.71	0.72	0.85	0.85	20.43	20.43	34.14	21.51	0.86	0.17	0.14	2.55	2.10	15.82	3.26
	19.53	0.82	0.46	0.46	11.02	11.02	30.54	11.75	0.80	0.26	0.22	5.19	4.15	23.68	5.91
	14.83	0.69	0.74	0.74	17.55	17.55	32.38	18.71	0.84	0.18	0.12	2.82	1.84	16.67	3.50
	18.86	0.62	0.36	0.31	7.31	6.04	24.91	8.53	0.87	0.17	-0.08	3.15	-2.04	16.83	4.27
	21.17	0.59	0.28	0.17	6.05	3.11	24.28	7.05	0.80	0.25	-0.21	5.13	-4.48	16.69	6.52
	18.11	0.68	0.33	0.31	7.11	6.77	24.88	8.18	0.77	0.24	-0.23	4.12	-3.92	14.19	5.10
	19.35	0.51	0.53	0.52	14.21	14.14	33.49	16.97	0.87	0.13	-0.01	2.42	-0.27	19.10	3.13
	18.76	0.63	0.42	0.41	9.15	8.99	27.74	10.51	0.82	0.16	-0.05	2.93	-1.27	17.47	3.96
	9.97	0.71	0.85	0.84	20.60	20.46	30.43	29.13	0.68	0.47	0.01	7.06	3.70	13.71	11.68
	11.96	0.70	0.65	0.63	12.92	12.19	24.15	16.95	0.63	0.56	-0.53	5.08	-4.69	6.78	7.35
	11.36	0.75	0.77	0.76	17.87	17.70	29.06	23.69	0.73	0.36	-0.19	4.12	-0.72	10.68	6.19
	10.36	0.81	0.80	0.80	17.47	17.39	27.75	23.36	0.76	0.31	-0.07	3.68	0.41	10.77	5.86
SAC	8.87	0.67	0.74	0.74	11.76	11.68	20.55	14.76	0.29	0.48	-0.42	3.63	-3.27	5.64	5.55
	9.96	0.74	0.60	0.59	9.96	9.79	19.74	12.90	0.69	0.24	-0.18	2.52	-2.02	7.94	4.24
	9.20	0.61	0.66	0.66	12.05	12.05	21.25	16.05	0.45	0.62	-0.60	4.39	-4.03	5.17	4.89
	9.93	0.58	0.62	0.61	10.62	10.48	20.41	13.84	0.52	0.31	-0.25	2.95	-2.36	7.56	4.06
	9.71	0.71	0.56	0.55	8.47	8.21	17.93	11.08	0.17	0.69	-0.69	5.33	-5.33	4.31	7.39
	10.54	0.78	0.31	-0.06	3.22	0.38	10.92	4.35	-0.07	1.15	-1.15	6.56	-6.56	2.39	6.85
	10.27	0.71	0.97	0.97	23.83	23.83	34.10	30.23	0.74	0.55	0.00	8.60	4.80	15.07	13.44
	9.50	0.73	0.64	0.63	11.30	11.20	20.70	15.31	0.70	0.53	-0.50	3.80	-3.12	6.38	4.85
	12.96	0.85	0.72	0.72	15.87	15.87	28.83	18.85	0.86	0.20	0.13	3.17	1.99	14.95	4.64
	10.94	0.83	0.83	0.83	18.43	18.43	29.37	22.90	0.88	0.21	0.07	3.02	1.81	12.75	5.10
	11.00	0.79	0.75	0.75	14.46	14.45	25.45	17.61	0.79	0.19	0.08	2.33	0.84	11.83	3.49
SFBA	10.41	0.75	0.47	0.45	7.70	7.37	17.77	10.74	0.30	0.61	-0.60	5.32	-5.29	5.11	7.67

The bias in CTM predictions at each monitoring location was combined with the CTM predicted concentrations of primary particles emitted from nine different source categories and the concentrations secondary nitrate and sulfate particulate matter to form a time-series that was analyzed using multi-linear regression (MLR) based on the equation

$$\text{Bias} = a_1*\text{Tracer1} + a_2*\text{Tracer2} + \ldots + a_9*\text{Tracer9} + a_{10}*\text{Nitrate} + a_{11}*\text{Sulfate} \quad \text{(eq 3)}$$

where a_i represents regression coefficients and $Tracer_i$ represents the concentrations of primary particles emitted from: 1. Onroad gasoline vehicles, 2. Offroad gasoline vehicles, 3. Onroad diesel vehicles, 4. Offroad diesel vehicles, 5. Biomass combustion, 6. Food cooking, 7. Aircraft, 8. Natural gas combustion, and 9. All other sources. Regression coefficients were constrained to values between -5 to +5 for sources other than aircraft and secondary nitrate / sulfate. Regression coefficients for aircraft were constrained to values between 0 to +5. A more limited range was necessary to prevent unreasonable correction factors in the vicinity of military air bases that do not have nearby measurement sites that would naturally constrain the coefficients.

The time series from all sites in central California were combined into a single dataset in order to support the eleven independent variables in the regression analysis. Results for all years were combined into a single regression for sites in central California because a single set of regression coefficients was able to explain the bias with an R^2=0.81 and a regression slop of 0.91. A separate yearly analysis was performed for the more numerous measurement sites in Los Angeles because the meteorological simulations in the South Coast Air Basin surrounding Los Angeles are somewhat separate from the meteorological simulations in the San Joaquin Valley due to the isolating effects of the mountain ranges between these locations. Results were analyzed for individual years in Los Angeles because the regression coefficients developed across all years had lower explanatory power, perhaps due to more significant changes to emissions over time.

The MLR bias equation (eq 3) was applied at each CTM grid cell to predict the bias in CTM concentrations. The baseline CTM concentrations were then adjusted using the equation

$$C^{bias\_corr} = C^{baseline} * (1\text{-}bias/C^{baseline}) \qquad \text{(eq 4)}$$

Bias corrections were only applied to primary PM components emitted directly to the atmosphere in the particle phase. Concentrations of secondary PM components predicted by the CTM were not adjusted because the measurements at the limited number of speciation sites suggested that secondary components were not over-predicted to the same extent as total mass.

Summary performance statistics comparing bias-corrected concentrations with measured values are shown on the right side of Table 5. MFB, MFE, ME, MB, and RMSQ improve at 34 out of 38 measurement locations, with average MFB= -0.17 for the bias corrected results (compared to MFB=0.56 for original results). These metrics indicate that the statistical bias correction removes a significant fraction of the over-prediction in the model results. Likewise, correlation coefficients (R^2) between bias-corrected predicted concentrations vs. measured concentrations improve at 20 out of 38 measurement sites, but degrade slightly at 13 sites and significantly at the remaining five sites (Figure 4). These summary statistics indicate that statistical bias correction generally improves the accuracy of the predicted exposure fields, but this method does not uniformly correct all errors in the CTM predictions, and may degrade performance at some locations. Future efforts should correct the bias in the transport calculations to reduce or eliminate the bias in the predicted concentration fields.

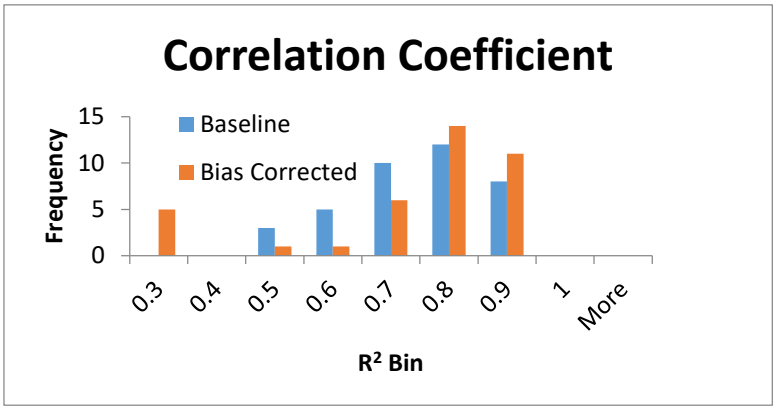

Figure 4: Correlation coefficient (R^2) between predicted and measured concentrations at 38 measurement sites across the 1-km domains shown in Figure 1.

3.2 PM2.5 Comparison to Measured Concentrations

Figures 5-8 illustrate the time trend of bias-corrected $PM_{2.5}$ predictions vs. measurements at 38 measurement locations across the four 1-km study domains. Predicted concentrations are largely in agreement with measured concentrations after bias-corrections following the methods described in the previous section.

A long-term trend of decreasing $PM_{2.5}$ concentrations is both predicted and observed across the measurements sites in the Los Angeles domain (Figures 5-6). The improvements in air quality are largely attributable to reductions in emissions motivated by State Implementation Plans (SIPs) designed to bring long-term concentrations into compliance with the National Ambient Air Quality Standards (NAAQS). Los Angeles is dominated by on-road vehicle emissions to a larger extent than other cities in California, and so improvements in fuel economy and emissions control systems are particularly noteworthy in this region. The adoption of new diesel engine standards in 2007 that require the use of diesel particle filters (DPFs) and ultra-low sulfur diesel (ULSD) fuel significantly reduced particulate matter emissions from heavy-duty vehicles in the Los Angeles region. Continuous improvements in Port Fuel Injection (PFI) engines decreased emissions from gasoline-powered light duty vehicles throughout the early 2000's, but the more recent adoption of Gas Direct Injection (GDI) engines in the light duty fleet has partially reversed this trend.

Figure 7 illustrates the time trend of bias-corrected $PM_{2.5}$ predictions vs. measurements across the San Francisco study domain. Greater amounts of residential wood combustion are used for winter home heating in central California compared to southern California, and so winter $PM_{2.5}$ concentrations are significantly higher than summer $PM_{2.5}$ concentrations in the San Francisco Bay Area. The Bay area Air Quality Management District (BAAQMD) adopted a wood burning device rule in 2008 corresponding to month 96 in Figure 7. These rules included no burn day advisories, use of cleaner burning devices, proper labeling of fire wood sold in the Bay Area, bans on burning of toxic substances and limitations on excessive burning. These rules contributed the a gradual decline in peak winter $PM_{2.5}$ concentrations across the SFBA.

Figure 8 illustrates the time trend of bias-corrected $PM_{2.5}$ predictions vs. measurements across the Sacramento and Fresno study areas. Major transportation corridors pass through each of these medium-sized cities, but they do not have the same degree of population density and traffic congestion that is experienced in Los Angeles and San Francisco. Sacramento and Fresno are also located in California Central Valley, which experiences colder temperatures during winter months compared to coastal cities. This emphasizes the trend of higher winter concentrations associated with residential home heating. The San Joaquin Valley Unified Air Pollution Control District implemented Rule 4901 to create more stringent controls on residential wood burning beginning in 2003. This rule applies to areas that are below 3,000 feet elevation with natural gas heating capabilities. An Environmental Health Evaluation submitted in 2008 showed the seasonal impact the rule made in reducing $PM_{2.5}$ concentrations in Fresno [33]. The Sacramento Metropolitan Air Quality Management District (SMAQMD) also enacted a curtailment program for wood burning. SMAQMD partnered with a local Low-Income Weatherization Program from 2008 to 2011 to fund installments of less polluting wood devices and gas stoves in low-income areas [34].

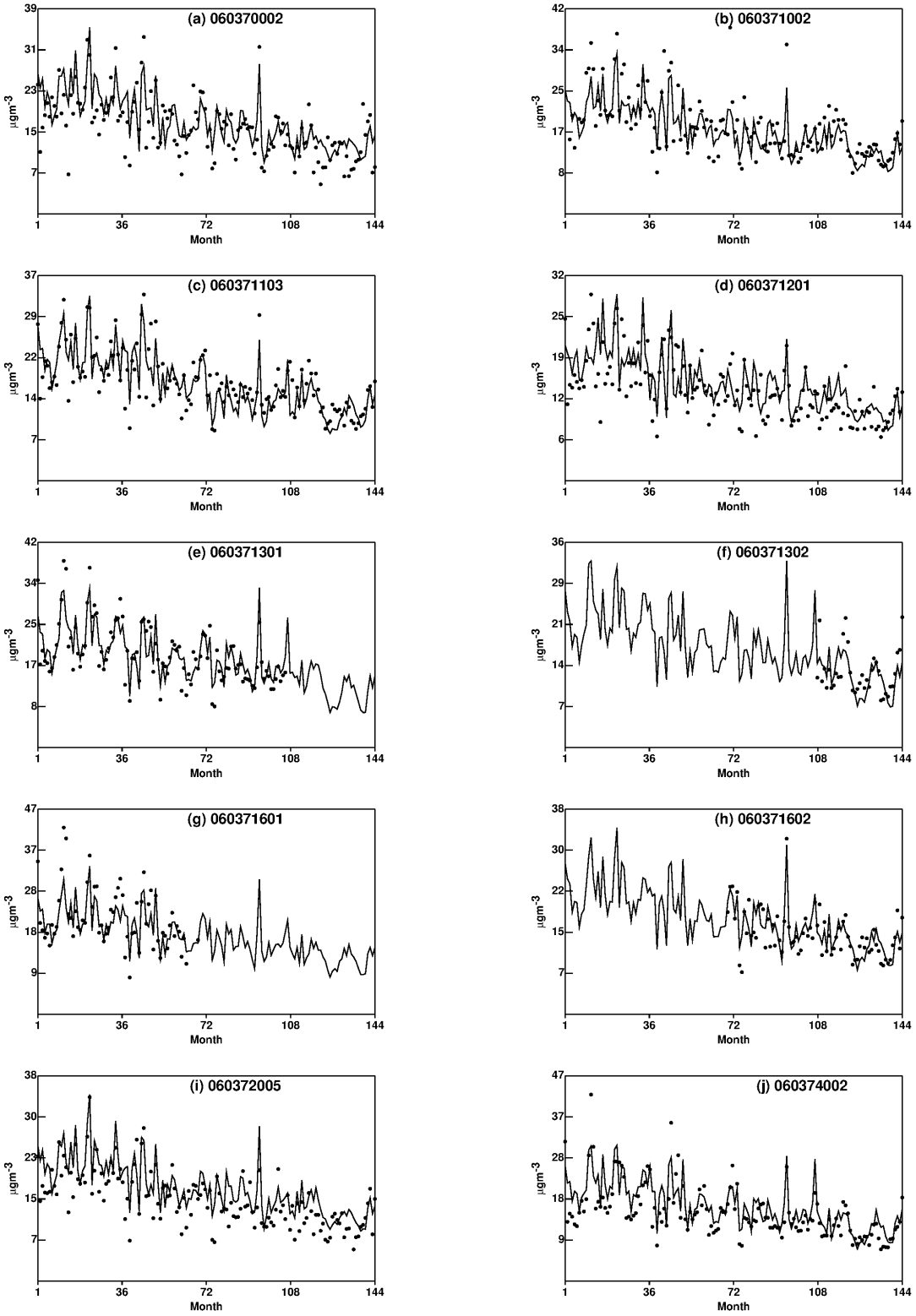

Figure 5: Time series of predicted (solid line) vs. measured (dots) monthly-average PM2.5 concentrations at measurement locations in the Los Angeles 1-km study region. All model concentrations have been bias-corrected. Measurement site codes correspond to names designated by the US EPA monitoring network.

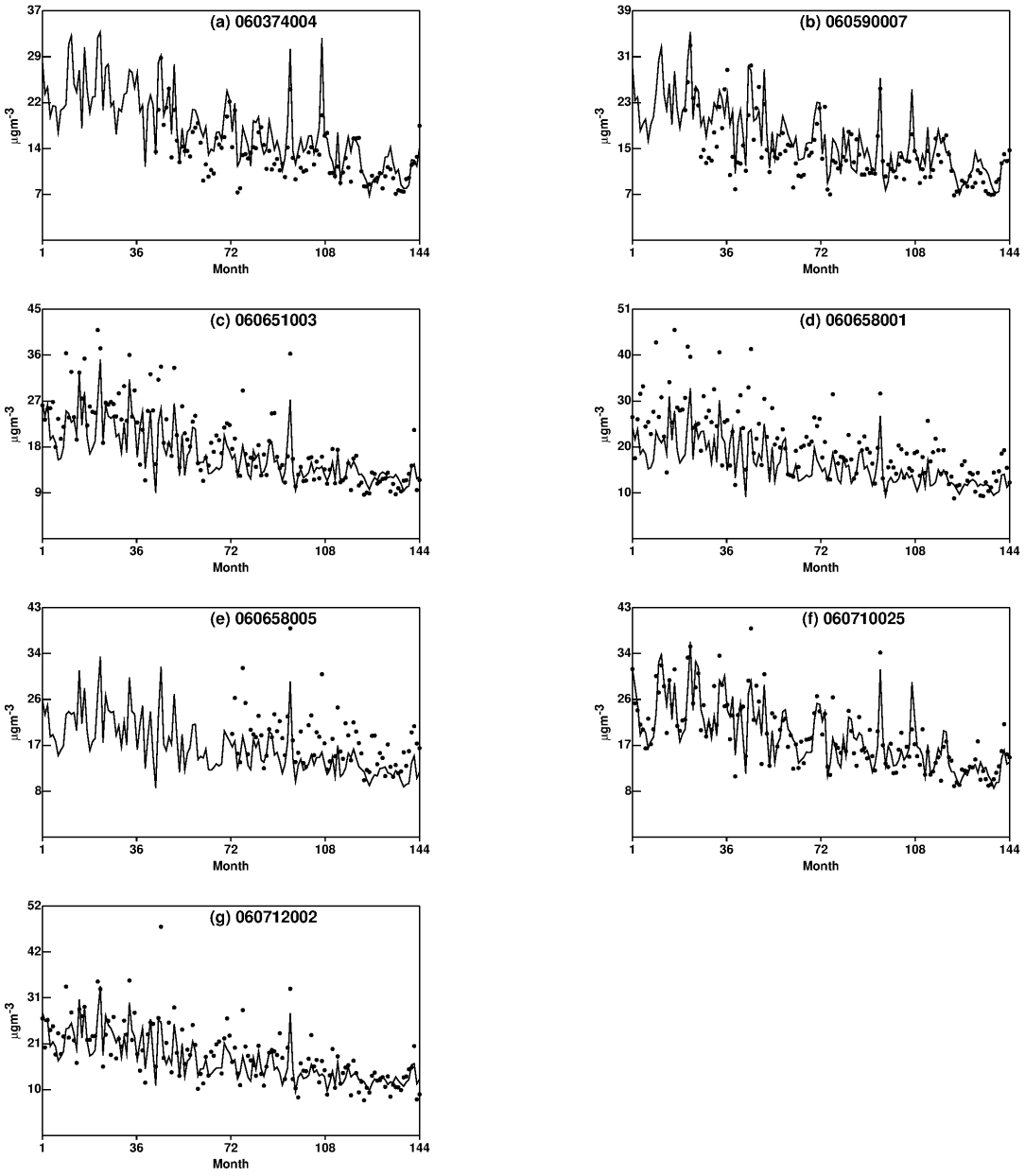

Figure 6: Time series of predicted (solid line) vs. measured (dots) monthly-average PM2.5 concentrations at measurement locations in the Los Angeles 1-km study region. All model concentrations have been bias-corrected. Measurement site codes correspond to names designated by the US EPA monitoring network.

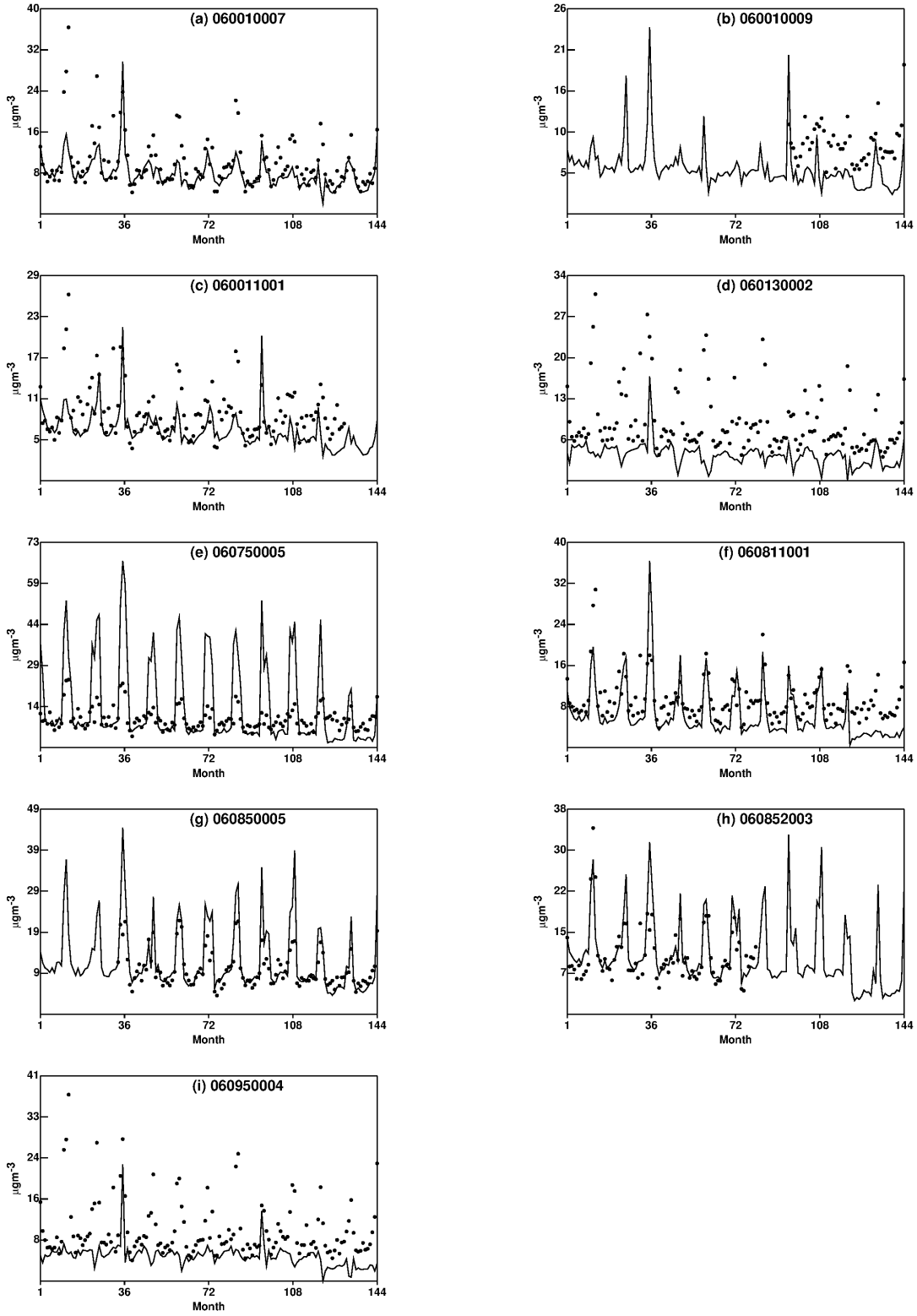

Figure 7: Time series of predicted (solid line) vs. measured (dots) monthly-average PM2.5 concentrations at measurement locations in the San Francisco Bay Area 1-km study region. All model concentrations have been bias-corrected. Measurement site codes correspond to names designated by the US EPA monitoring network.

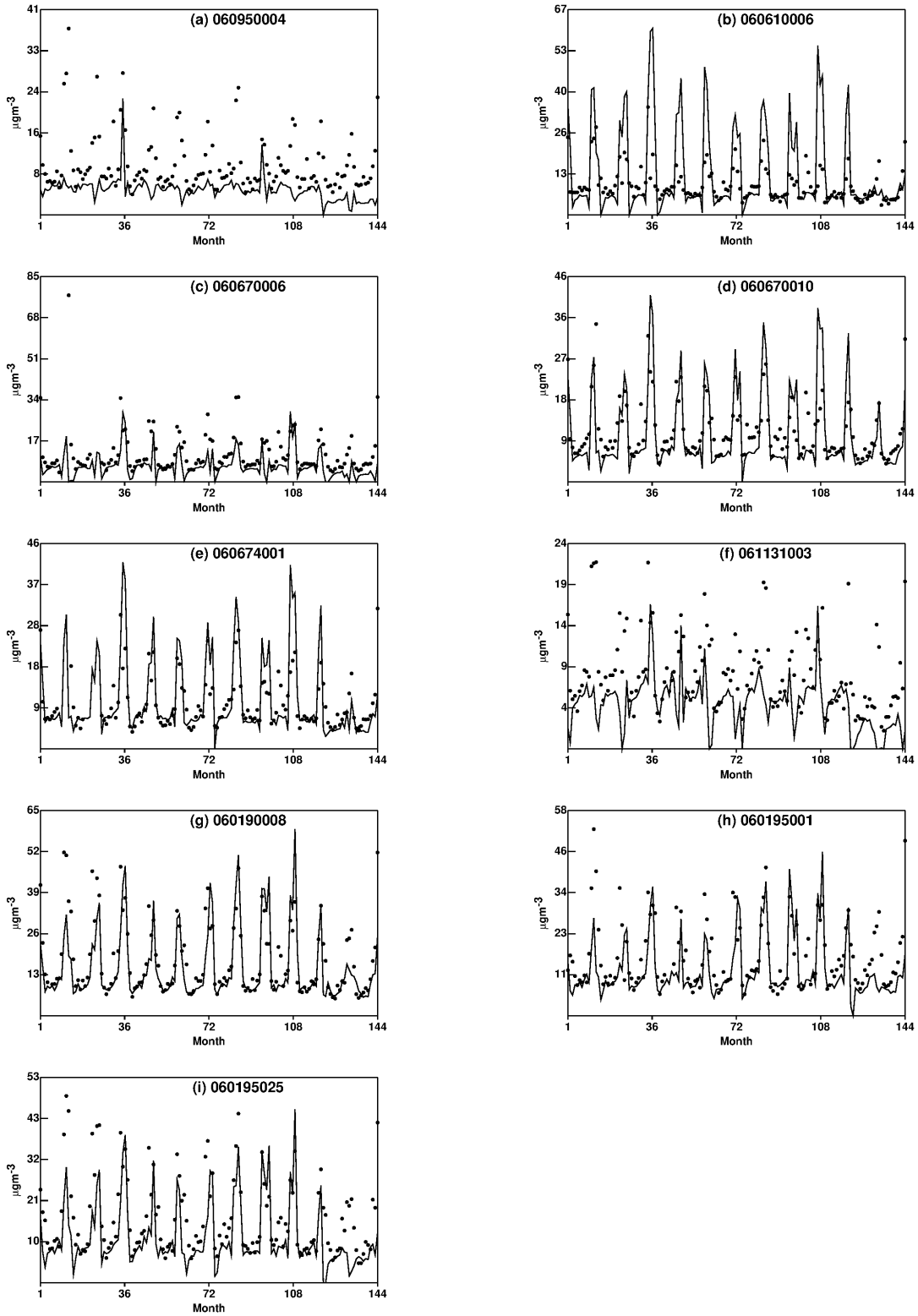

Figure 8: Time series of predicted (solid line) vs. measured (dots) monthly-average PM2.5 concentrations at measurement locations in the Sacramento (a-f) and Fresno (g-i) 1-km study regions. All model concentrations have been bias-corrected. Measurement site codes correspond to names designated by the US EPA monitoring network.

3.3 Spatial Plots of Exposure Fields

On-road vehicles emit primary particulate matter that contributes to the $PM_{2.5}$ concentrations across urban areas in California. Many other sources also emit particulate matter, including residential wood combustion, food cooking, agricultural activities, natural gas combustion, etc. The source-tagging features inherent in the CTM used to predict concentration fields in the current study was used to explicitly track tailpipe emissions through the simulation of atmospheric mixing, advection, deposition, and chemical reaction. These calculations capture the time and spatial trends in motor vehicle emissions that are needed for public health assessments.

Figure 9 shows the spatial distribution of predicted $PM_{2.5}$ mass concentrations averaged over the years 2000-2011 after statistical bias correction. Each panel of Figure 9 illustrates results for a different region of California with different spatial resolution. Figure 9a illustrates results covering all of California with 24-km spatial resolution, with highest concentrations generally predicted in Los Angeles and throughout the Central Valley. Figures 9b and 9c illustrate predicted $PM_{2.5}$ concentrations over the San Joaquin Valley and the South Coast Air Basin with 4-km spatial resolution. Figures 9d, 9e, and 9f illustrate predicted $PM_{2.5}$ concentrations over Sacramento, the San Francisco Bay Area, Fresno, and Los Angeles with 1-km spatial resolution. The increased spatial resolution brings features of the pollution fields into focus that are hidden at the coarse spatial resolution. Transportation corridors are apparent in several of the high-resolution 1-km fields but are masked from view in the 4-km and 24-km fields.

Figure 10 shows the spatial distribution of predicted $PM_{2.5}$ EC concentrations averaged over the years 2000-2011 using the same format as Figure 9. EC is a sub-component of $PM_{2.5}$ mass that is often associated with traffic sources. $PM_{2.5}$ EC concentrations are lower than total $PM_{2.5}$ mass concentrations, and the spatial gradients in the $PM_{2.5}$ EC fields are sharper. Both on-road and off-road diesel engines contribute strongly to $PM_{2.5}$ EC concentrations, with the highest concentrations predicted at shipping ports associated directly with ships themselves or the equipment used to service ships.

Figures 11 and 12 show the spatial distribution of primary $PM_{2.5}$ mass emitted from on-road gasoline engines, and on-road diesel engines, respectively. Maximum concentrations from on-road sources are generally less than 5% of total $PM_{2.5}$ mass concentrations. Secondary particulate matter produced from precursor gases emitted from motor vehicles adds to this total but are not quantified in the current study. Likewise, road dust, tire wear, and brake wear particulate matter are included as part of the total $PM_{2.5}$ mass shown in Figure 9 and are not included in Figures 11 and 12. The concentration fields for gasoline and diesel vehicles generally reflect the activity patterns of freight transport and passenger vehicles. Freight transport is focused on major highways leading to and from shipping ports or regional warehouses. Passenger vehicle traffic is more evenly distributed across the major transportation facilities spanning urban areas. All of these features are apparent at 1-km spatial resolution but somewhat masked at 4-km and 24-km spatial resolution.

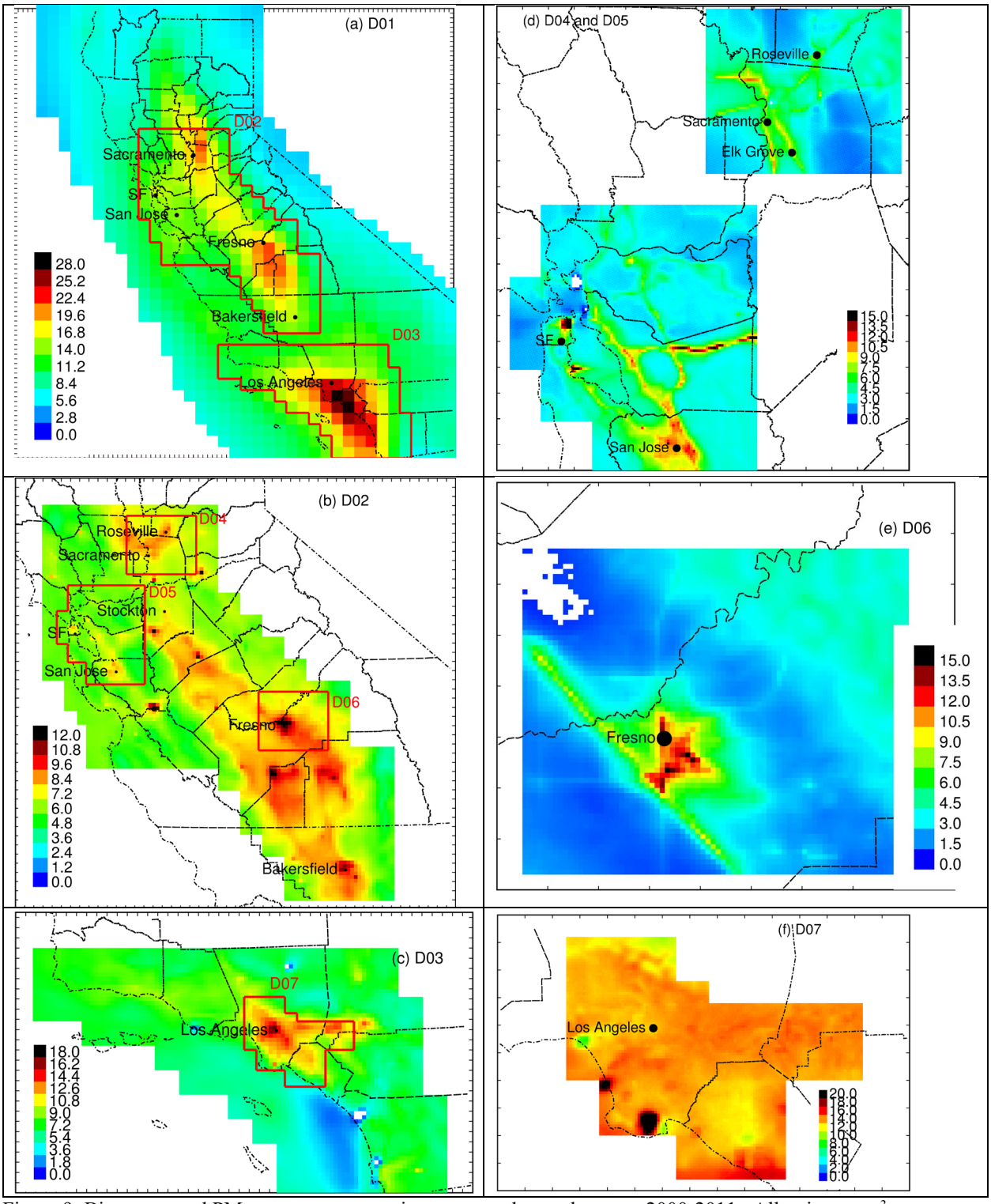

Figure 9: Bias-corrected $PM_{2.5}$ mass concentrations averaged over the years 2000-2011. All units μg m^{-3}.

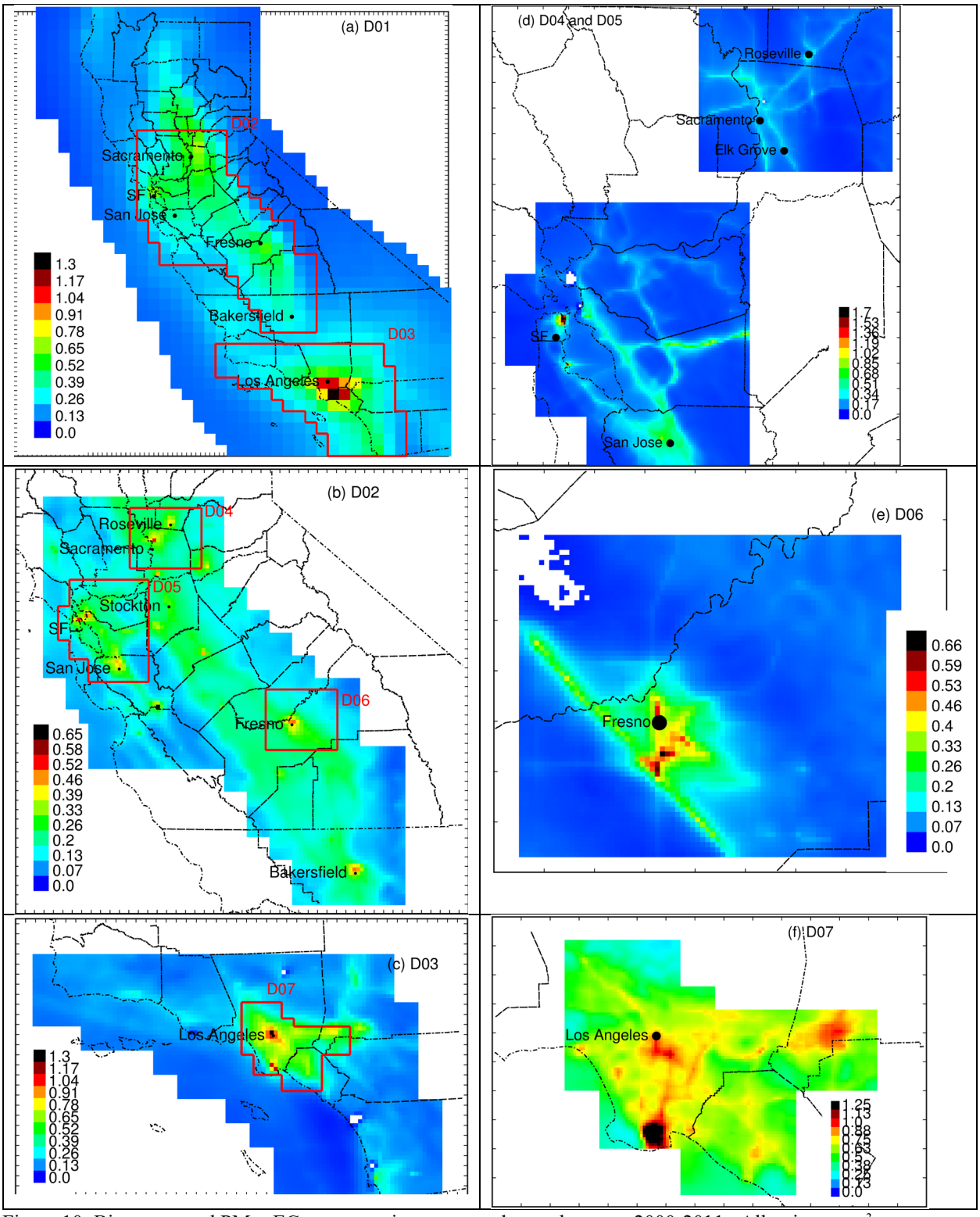

Figure 10: Bias-corrected $PM_{2.5}$ EC concentrations averaged over the years 2000-2011. All units μg m^{-3}.

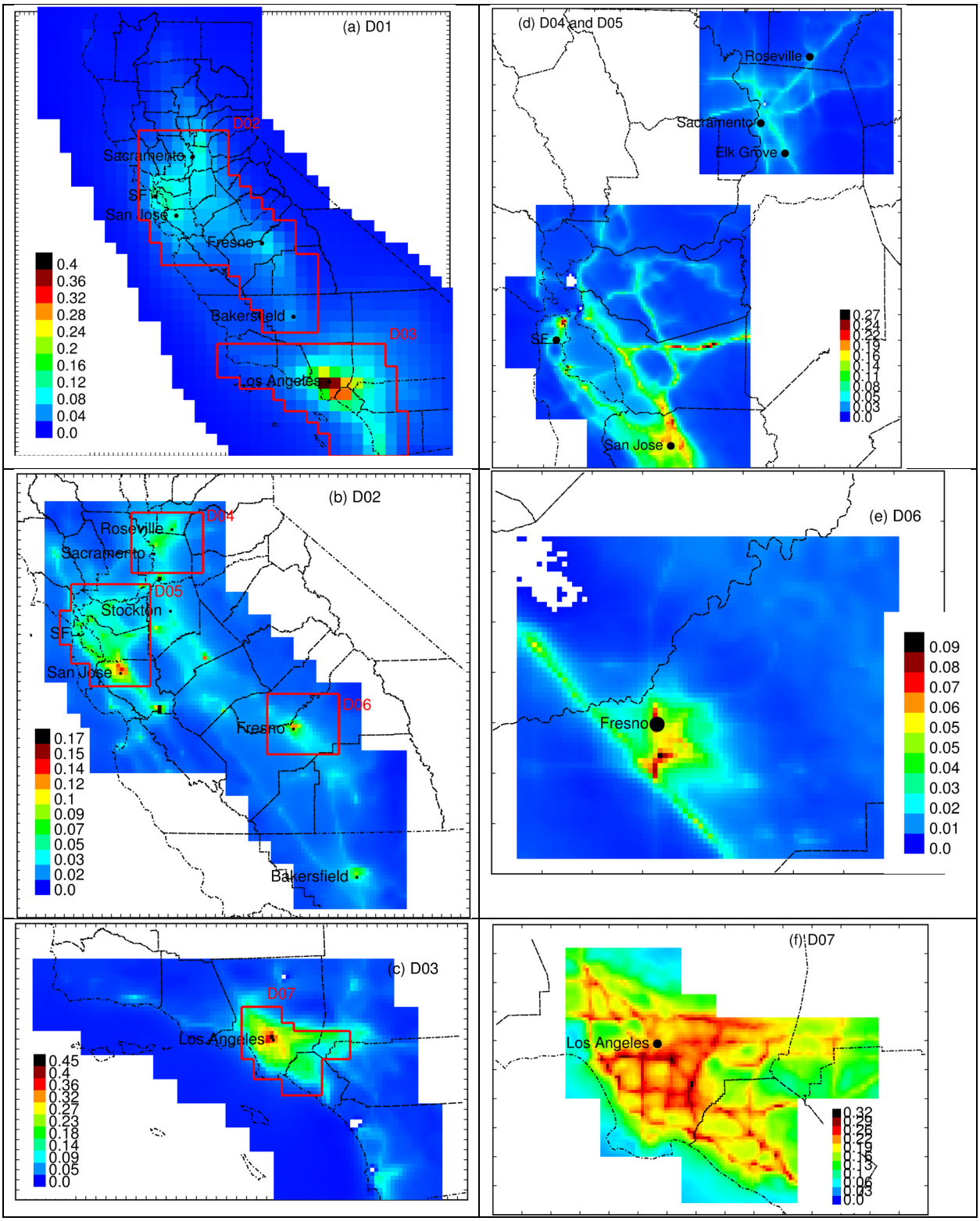

Figure 11: Bias-corrected $PM_{2.5}$ mass concentrations associated with on-road gasoline vehicles averaged over the years 2000-2011. All units μg m^{-3}.

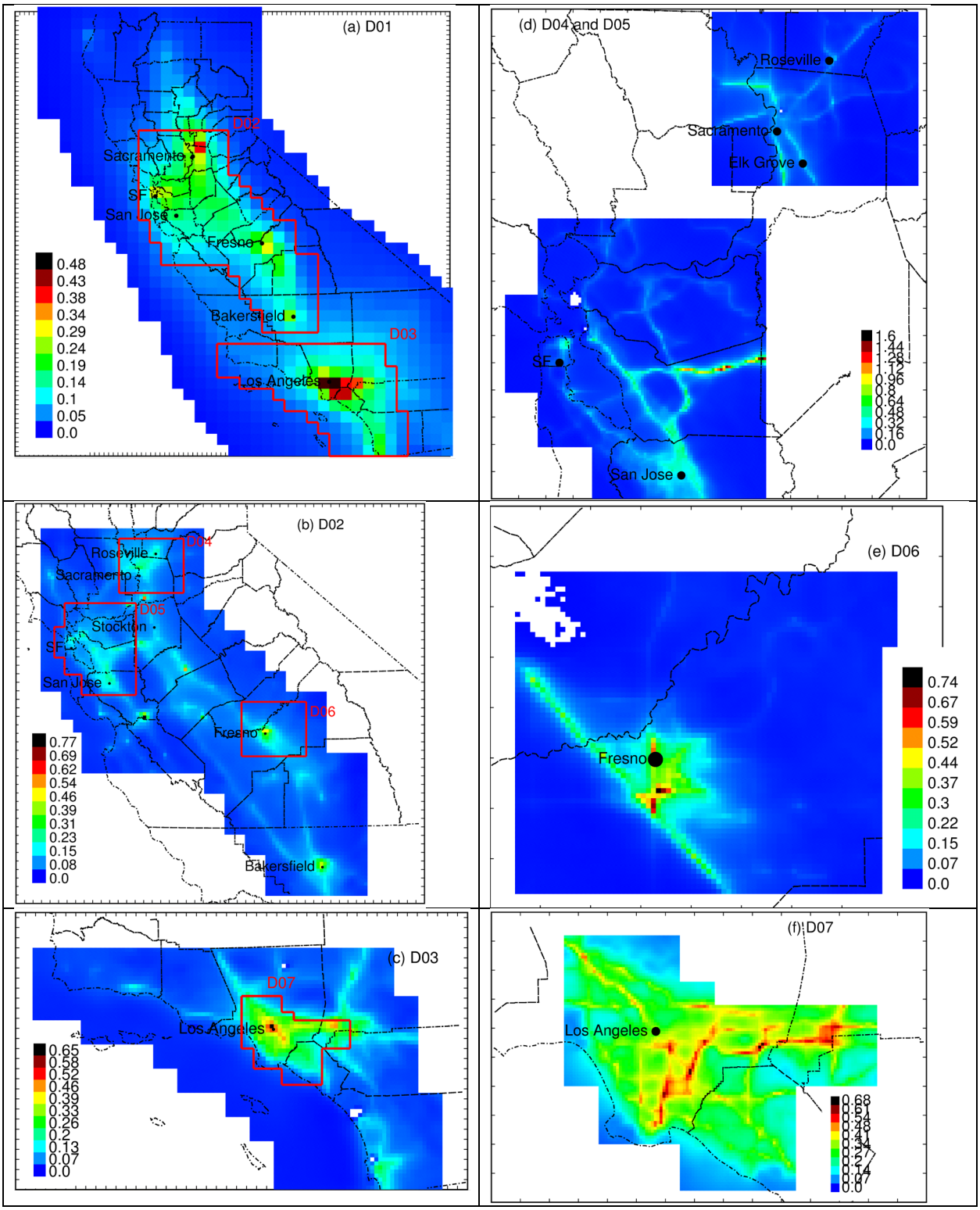

Figure 12: Bias-corrected $PM_{2.5}$ mass concentrations associated with on-road diesel vehicles averaged over the years 2000-2011. All units μg m^{-3}.

3.4 Public Health Impacts of Tailpipe Emissions

The public health impacts of total $PM_{2.5}$ mass concentrations and $PM_{2.5}$ mass concentrations associated with on-road motor vehicles were calculated using the BenMAP-CE v1.5 model provided by the US EPA(Sacks et al., 2018). The $PM_{2.5}$ health impact function was taken from a major epidemiological study (Pope et al., 2002). Avoided mortality was translated to a monetary value using the standard value of a statistical life (VSL) recommended by US EPA yielding a VSL equivalent to USD 7.6 M. The spatial distribution of population assumed in health impact calculations was based on 2010 census information, which is consistent with the assumptions inherent when creating the 1-km emissions inventories for on-road vehicles. Mortality calculations for total $PM_{2.5}$ mass assume a uniform background concentration of 3 $\mu g\ m^{-3}$, while mortality calculations for $PM_{2.5}$ mass associated with on-road motor vehicles assume a background concentration of 0 $\mu g\ m^{-3}$.

Figure 13a shows the predicted mortality trends for the 1-km Los Angeles study region between the years 2000-2011. Total $PM_{2.5}$ mortality generally declines over this time period due to the decreasing ambient $PM_{2.5}$ mass concentrations across the region (see Figures 5-6 and associated discussion). $PM_{2.5}$ mortality associated with on-road motor vehicles accounts for less than 5% of the total $PM_{2.5}$ mortality due to the relatively low contribution that tailpipe emissions make to total $PM_{2.5}$ concentrations. $PM_{2.5}$ mortality associated with on-road motor vehicles generally declines along with the total $PM_{2.5}$ mortality except during the final two years of the study period.

Figures 13b and 13c show the predicted $PM_{2.5}$ mortality trends for the San Francisco and Sacramento study domains, respectively. $PM_{2.5}$ mortality associated with on-road sources once again account for less than 5% of total $PM_{2.5}$ mortality in these study regions. Both total $PM_{2.5}$ mortality and on-road vehicle $PM_{2.5}$ mortality decline over time due to reduced ambient $PM_{2.5}$ concentrations.

Figure 13d shows the predicted $PM_{2.5}$ mortality trends for Fresno. Long term trends in $PM_{2.5}$ mortality are not as apparent in this study domain as they are in the other three domains. This constant behavior reflects the general lack of change in ambient $PM_{2.5}$ concentrations in Fresno during the study time period (see Figure 8g-i).

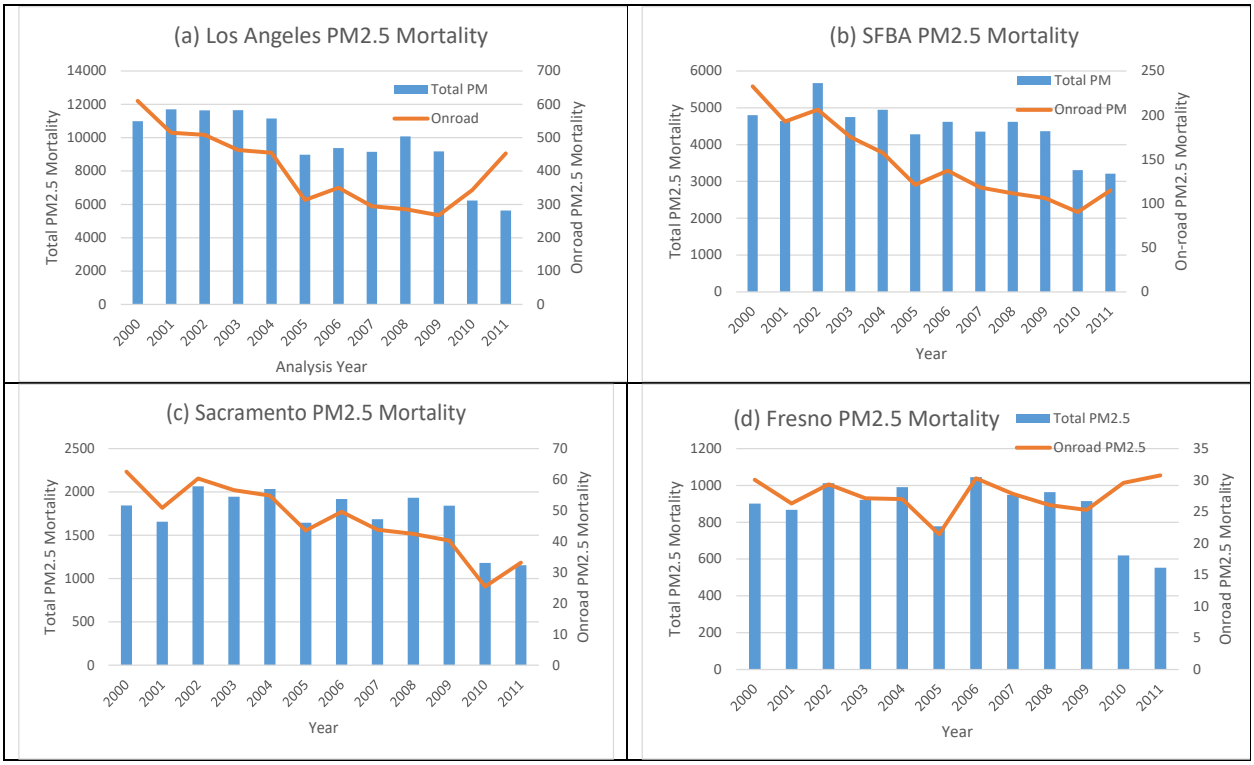

Figure 13: Mortality associated with total $PM_{2.5}$ mass concentrations and $PM_{2.5}$ mass emitted from on-road vehicles.

The monetary value of the public health penalty associated with exposure to $PM_{2.5}$ concentrations can be calculated by multiplying the mortality values displayed in Figure 13 with the Value of a Statistical Life recommended by the US EPA ($7.6M). Using these figures, the total $PM_{2.5}$ penalty decreased by $40B yr^{-1} (Los Angeles), $12B yr^{-1} (San Francisco), $5B yr^{-1} (Sacramento), and $2.6B yr^{-1} (Fresno). On-road vehicles accounted for $1.2B yr^{-1} (Los Angeles), $890M yr^{-1} (San Francisco), and $220M yr^{-1} (Sacramento) of these public health savings. Fresno is predicted to suffer from increased $PM_{2.5}$ concentrations associated with on-road motor vehicles during the study period, with an additional public health burden equivalent to $5B yr^{-1}.

4 Conclusions

The development of pollutant concentration fields with 1-km spatial resolution helps bring $PM_{2.5}$ spatial gradients around major transportation corridors across California into focus. These pollutant fields can be used for more accurate calculations for public health impacts from on-road vehicles compared to coarser fields developed at 4-km or 24-km spatial resolution.

$PM_{2.5}$ total mass concentrations decreased across Los Angeles, the San Francisco Bay Area, and Sacramento during the period 2000 – 2011. Long-term reduction trends were less obvious at Fresno during the same time period. The improvement to air quality can largely be attributed to reduced emissions from on-road vehicles, and the adoption of curtailments on winter wood burning for home heating. Trends for $PM_{2.5}$ mass concentrations associated with on-road motor vehicles largely mirror trends in total $PM_{2.5}$ mass concentrations. Specific measures leading to reduced $PM_{2.5}$ mass concentrations associated with on-road vehicles include adoption of Diesel Particle Filters (DPFs) and continuous improvements in gasoline vehicle engines over the study time period.

The public health benefits associated with reduced emissions from motor vehicle traffic can be expressed as 300 avoided deaths each year with an equivalent monetary value estimated at $2.3B yr^{-1} using standard account methods published by the US EPA.

5 Future Work

The pollutant fields developed in the current project should be useful for a number of follow-on studies. Demographic information may be used to quantify any disparities in the public health burden associated with exposure to traffic related air pollution based on race or income level. Epidemiological studies may be conducted using the exposure fields to identify associations with numerous health endpoints (death, diabetes, cognitive impairment, overall physical fitness, autism, learning disabilities, etc). All of the pollutant concentration fields developed under the current project are available to the public at www.archive.address.

6 Acknowledgements

The contents of this report reflect the views of the authors, who are responsible for the facts and the accuracy of the information presented herein. This document is disseminated in the interest of information exchange. The report is funded, partially or entirely, by a grant from the U.S. Department of Transportation's University Transportation Centers Program. However, the U.S. Government assumes no liability for the contents or use thereof.

7 References

1. Held, T., et al., *A comparision of the UCD/CIT air quality model and the CMB source-receptor model for primary airborne particulate matter.* Atmospheric Enviornment, 2005. **39**: p. 2281-2297.
2. Hu, X.-M., et al., *Coupling and evaluating gas/particle mass transfer treatements for aerosol simulation and forecast.* J. Geophys. Res., 2008. **113**(D11208).
3. Nenes, A., C. Pilinis, and S.N. Pandis, *ISORROPIA: A new thermodynamic equilibrium model for multiphase multicomponent marine aerosols* Aquat. Geochem, 1998. **4**: p. 123-152.
4. Carlton, A.G., et al., *Model representation of secondary organic aerosol in CMAQv4.7.* Environmental Science and Technology, 2010. **44**: p. 8553-8560.

5. Kleeman, M.J., G.R. Cass, and A. Eldering, *Modeling the airborne particle complex as a source-oriented external mixture.* Journal of Geophysical Research-Atmospheres, 1997. **102**(D17): p. 21355-21372.
6. Ying, Q., et al., *Modeling air quality during the California Regional PM10/PM2.5 Air Quality Study (CRPAQS) using the UCD/CIT source-oriented air quality model - Part I. Base case model results.* Atmospheric Environment, 2008. **42**(39): p. 8954-8966.
7. Hu, J., et al., *Long-term particulate matter modeling for health effect studies in California – Part 1: Model performance on temporal and spatial variations.* Atmospheric Chemistry and Physics, 2015. **15**(6): p. 3445-3461.
8. Yu, X., et al., *Sources of Airborne Ultrafine Particle Number and Mass Concentrations in California.* Atmos. Chem. Phys. Discuss., 2018. **2018**: p. 1-37.
9. Ying, Q., et al., *Modeling air quality during the California Regional PM10/PM2.5 Air Quality Study (CPRAQS) using the UCD/CIT Source Oriented Air Quality Model - Part II. Regional source apportionment of primary airborne particulate matter.* Atmospheric Environment, 2008. **42**(39): p. 8967-8978.
10. Ying, Q., et al., *Verification of a source-oriented externally mixed air quality model during a severe photochemical smog episode.* Atmospheric Environment, 2007. **41**(7): p. 1521-1538.
11. Carter, W.P.L. and G. Heo, *Development of Revised SAPRC Aromatics Mechanisms.* Atmospheric Environment, 2013. **77**: p. 404-414.
12. Hong, S.Y., Y. Noh, and J. Dudhia, *A new vertical diffusion package with an explicit treatment of entrainment processes.* Monthly Weather Review, 2006. **134**(9): p. 2318-2341.
13. Xiu, A.J. and J.E. Pleim, *Development of a land surface model. Part I: Application in a mesoscale meteorological model.* Journal of Applied Meteorology, 2001. **40**(2): p. 192-209.
14. Su, L. and J.C.H. Fung, *Sensitivities of WRF-Chem to dust emission schemes and land surface properties in simulating dust cycles during springtime over East Asia.* Journal of Geophysical Research-Atmospheres, 2015. **120**(21): p. 11215-11230.
15. United States Department of Health and Human Services (US DHHS), Centers for Disease Control and Prevention (CDC), and National Center for Health Statistics (NCHS), *Compressed Mortality File (CMF) 1999-2013 with ICD-10 Codes on on CDC WONDER Online Database.*, in *The current release for years 1999 - 2013 is compiled from: CMF 1999-2013, Series 20, No. 2S, 2014.* 2014.
16. Hu, J., et al., *Predicting primary PM2.5 and PM0.1 trace composition for epidemiological studies in California.* Environ Sci Technol, 2014. **48**(9): p. 4971-9.
17. McDonald, B.C., et al., *High-resolution mapping of motor vehicle carbon dioxide emissions.* Journal of Geophysical Research-Atmospheres, 2014. **119**(9): p. 5283-5298.
18. McDonald, B.C., et al., *Long-Term Trends in Motor Vehicle Emissions in US Urban Areas.* Environmental Science & Technology, 2013. **47**(17): p. 10022-10031.
19. Gentner, D.R., et al., *Elucidating secondary organic aerosol from diesel and gasoline vehicles through detailed characterization of organic carbon emissions.* Proceedings of the National Academy of Sciences of the United States of America, 2012. **109**(45): p. 18318-18323.
20. Dallmann, T.R., et al., *Quantifying On-Road Emissions from Gasoline-Powered Motor Vehicles: Accounting for the Presence of Medium- and Heavy-Duty Diesel Trucks.* Environmental Science & Technology, 2013. **47**(23): p. 13873-13881.
21. Dallmann, T.R., et al., *On-Road Measurement of Gas and Particle Phase Pollutant Emission Factors for Individual Heavy-Duty Diesel Trucks.* Environmental Science & Technology, 2012. **46**(15): p. 8511-8518.
22. Herner, J.D., et al., *Effect of Advanced Aftertreatment for PM and NOx Control on Heavy-Duty Diesel Truck Emissions.* Environmental Science & Technology, 2009. **43**(15): p. 5928-5933.
23. Xue, J., et al., *Seasonal and annual source appointment of carbonaceous ultrafine particulate matter (PM0.1) in polluted California cities.* Environmental Science & Technology, 2018. **in review**.
24. Xue, J., et al., *Ultrafine particle emissions from natural gas, biogas and biomethane combustion.* Environmental Science & Technology, 2018. **in press**.
25. Almaraz, M., et al., *Agriculture is a major source of NOx pollution in California.* Science Advances, 2018. **4**(1).
26. Kleeman, M., A. Kumar, and A. Dhiman, *Investigative Modeling of PM2.5 Episodes in the San Joaquin Valley Air Basin during Recent Years*. 2018, California Air Resources Board Research Division Report # 15-301.

27. Guenther, A.B., et al., *The Model of Emissions of Gases and Aerosols from Nature version 2.1 (MEGAN2.1): an extended and updated framework modeling biogenic emissions.* Geoscientific Model Development, 2012. **5**: p. 1471-1492.
28. Giglio, L., J.T. Randerson, and G.R. van der Werf, *Analysis of daily, monthly and annual burned area using the fourth-generation global fire emissions database (GFED4).* Journal of Geophysical Research, 2013. **118**(1): p. 317-328.
29. Paugam, R., et al., *A review of approaches to estimate wildfire plume injection height within large-scale atmospheric chemical transport models.* Atmospheric Chemistry and Physics, 2016. **16**(2): p. 907-925.
30. van der Werf, G.R., et al., *Global fire emissions estimates during 1997-2016.* Earth System Science Data, 2017. **9**(2): p. 697-720.
31. Hays, M.D., et al., *Open burning of agricultural biomass: Physical and chemical properties of particle-phase emissions.* Atmospheric Environment, 2005. **39**(36): p. 6747-6764.
32. Emmons, L., et al., *Description and evaluation of the Model for Ozone and Related chemical Tracers, version 4 (MOZART-4).* Geoscientific Model Development, 2010. **3**(1): p. 43-67.
33. Lighthall, D., Nunes, D., Tyner, T., *Environmental Health Effects of Rule 4901: Domestic Wood Burning*. 2008, Central Valley Health Policy Institute, Central California Center for Health and Human Services, College of Health and Human Services, California State University Fresno.
34. EPA, *Strategies for Reducing Residential Woodsmoke*. 2013.